

## RESEARCH ARTICLE

# In vitro characterization of bionanocomposites with green silver nanoparticles: A step towards sustainable wound healing materials

Federico Trotta<sup>1</sup>  | Alna Dony<sup>1</sup> | Monica Mok<sup>1</sup> | Alessandra Grillo<sup>2</sup> | Thomas Whitehead-Clarke<sup>2</sup> | Shervanthi Homer-Vanniasinkam<sup>3</sup> | Alvena Kureshi<sup>2</sup> 

<sup>1</sup>Metalchemy Limited, London, UK

<sup>2</sup>Centre for 3D Models of Health and Disease, Division of Surgery and Interventional Science, University College London, London, UK

<sup>3</sup>Department of Mechanical Engineering, University College London, London, UK

## Correspondence

Federico Trotta, Metalchemy Limited, 71–75 Shelton Street, London, WC2H 9JQ, UK.

Email: [ft@metalchemy.tech](mailto:ft@metalchemy.tech)

Alvena Kureshi, Centre for 3D Models of Health and Disease, Division of Surgery and Interventional Science, University College London, Charles Bell House, Foley Street, London, W1W 7TY, UK.

Email: [a.kureshi@ucl.ac.uk](mailto:a.kureshi@ucl.ac.uk)

## Funding information

University College London

## Abstract

This study investigated the characterization, antifungal activity, and biocompatibility of green agar/silver and collagen/silver bionanocomposite films for wound healing and cell growth scaffolds. Silver nanoparticles (AgNPs) are known for their antimicrobial properties, but their toxicity and harsh synthesis limit their applications. To address this, green-synthesized AgNPs G-AgNPs were incorporated into agar/collagen suspensions at specific concentrations and three different G-AgNP-agar and two different G-AgNP-col bionanocomposite films were produced. Nanoparticle homogeneity and film quality were characterized through SEM analysis. Mechanical properties were tested using a uniaxial tensile tester, revealing that the bioplastic control samples exhibited UTS of 3.86 MPa compared to 0.60 MPa for collagen, a 6-fold improvement. Viable cell metabolic activity derived from MTT assay showed that Col-4%AgNPs and Bio-30%AgNPs had a 42.9% and 51.6% increase in net metabolic activity respectively compared to control on day 4. Fluorescence microscopy confirmed enhanced cell adhesion and proliferation in G-AgNP-incorporated samples. Antifungal properties were evaluated against *Cladosporium* spores, able to cause severe diseases when in contact with human skins, following ISO 16869:2008 standards. The demonstrated unique properties and tunability of G-AgNPs bionanocomposites can be employed in a variety of specialties for wound-healing applications, to improve rate and quality of healing while reducing the risk of infection.

## KEYWORDS

bionanocomposite, colloidal silver, green-chemistry, silver nanoparticles, sustainable biomaterials, tissue engineering, wound-healing

## 1 | INTRODUCTION

Chronic and recurrent wounds present a significant global healthcare burden.<sup>[1]</sup> With the global advanced wound

care market being projected to reach \$18.7 billion by 2027, in the UK alone, the annual cost for wound management in the UK for the National Health Service (NHS) is a staggering \$6.5 billion<sup>[1,2]</sup> – demonstrating a need for frugal

This is an open access article under the terms of the [Creative Commons Attribution](https://creativecommons.org/licenses/by/4.0/) License, which permits use, distribution and reproduction in any medium, provided the original work is properly cited.

© 2023 The Authors. *Nano Select* published by Wiley-VCH GmbH.

TABLE 1 Summary of advantages and disadvantages of current biomaterials used in wound dressings.<sup>[8]</sup>

Biomaterials	Advantages	Disadvantages
Cellulose/Agar-Agar	<ul style="list-style-type: none"> <li>Carboxymethyl cellulose &amp; Agar-Agar (CMC) has high abundance and low cost – making it ideal for sustainable, frugal innovation.</li> <li>CMC is very hydrophilic, increasing the ability of CMC hydrogels to absorb wound exudate and provide a moist environment to prevent loss of moisture around the wound.</li> </ul>	<ul style="list-style-type: none"> <li>CMC has relatively poor cell adhesion.</li> <li>Lack of antimicrobial activity is observed with CMC and BC hydrogels.</li> <li>The hydrophilic nature of CMC results in poor water stability, making it less durable as a wound-dressing.</li> </ul>
Collagen	<ul style="list-style-type: none"> <li>Collagen is the main component of the extracellular matrix in animals, and exhibits strong biocompatibility, biodegradability, and water stability.</li> <li>When used in wound-dressings, collagen promotes cell growth and proliferation, haemostasis and reduces scar formation – hence improving the rate and quality of healing.</li> </ul>	<ul style="list-style-type: none"> <li>Poor mechanical properties are currently the main limitation of collagen hydrogels, as well as a lack of antimicrobial activity. However, these aspects can be overcome by incorporating other green additives.</li> <li>High cost and low tunability.</li> </ul>

methods of improving wound care to reduce this worldwide burden and improve the rate of healing. Pain and discomfort, and well as reduced mobility from chronic wounds have been shown to be related to anxiety and depression in patients, resulting in significantly reduced quality of life.<sup>[3]</sup> Hence, improved wound-healing strategies have the potential to transform patient experiences and allow for improved quality of life in those experiencing chronic wounds. In addition to this, surgical wounds (\$1.2 billion), diabetic ulcers (\$674 million) and pressure ulcers (\$646 million) posed the greatest costs for healing for the NHS,<sup>[2]</sup> suggesting that new strategies are required to reduce heavy resource consumption through accelerating and optimizing the rate of healing for both acute and chronic wounds.

Table 1 shows the commonly used natural biomaterials for wound-healing. Following the establishment of the “17 Goals for Sustainable Development” by the United Nations, there is a strong incentive to transition to cleaner, green processes in manufacturing and sustainable consumption of resources – both of which are particularly relevant within the healthcare industry where resources are scarce.<sup>[4]</sup> While agar and cellulose components are less effective when used alone in hydrogels, when combined with other natural additives to produce bioplastics – the mechanical properties can be significantly improved, with increased strength and extensibility.<sup>[5]</sup> In addition to this, whilst collagen hydrogels provide an effective environment for wound healing,<sup>[6]</sup> current uses do not conventionally use green silver nanoparticles within its matrix as a method of imparting the material with antimicrobial properties and tunable mechanical properties, paving a path to evade the main short-coming of collagen scaffolds.<sup>[7]</sup>

Current methods of obtaining silver nanoparticles use toxic and expensive chemicals as reducing agents – making their use both expensive and damaging for the

environment.<sup>[9]</sup> These conventional methods act through reduction of silver ions with NaBH<sub>4</sub>, a toxic chemical that has negative health and environmental impacts.<sup>[10]</sup> By employing a green synthesis route, we can obtain green silver nanoparticles (G-AgNPs) in a safer and more sustainable method. Due to the low efficiency and high-cost of most current green synthesis methods, they are not commercially available in industry, with green synthesis reactions taking over 6 hours to complete.<sup>[11]</sup> However, recent developments have established a low cost, efficient and non-toxic process to produce G-AgNPs (green silver nanoparticles), taking 5–10 minutes to complete and demonstrating a 36 to 72-fold improvement in efficiency.<sup>[12]</sup>

AgNPs have been used in a variety of sectors including in healthcare due to their excellent antimicrobial properties.<sup>[4]</sup> It is well understood that antimicrobial colonization of wounds is a risk factor for poor tissue healing, with Gram-positive bacteria such as *Staphylococcus aureus*, *Escherichia coli*, and *Pseudomonas aeruginosa* being found to be the predominant pathogens – of which the incidence of multi-resistant strains continues to increase. It has been established that the use of AgNPs and their antimicrobial activity may contribute to reducing microbial infection and aid the later stages of healing.<sup>[13]</sup> Although the well-known antimicrobial actions, AgNPs antifungal activities still remain less investigated. Indeed, fungal species such as *Candida albicans*,<sup>[14]</sup> *Tinea versicolor*,<sup>[15]</sup> and *Cladosporium*<sup>[16]</sup> can cause severe skin diseases in humans. For instance, wound necrosis was linked to the detection of disease-causing fungal species like *Candida*.<sup>[17]</sup> When wound biofilms were directly cultured, yeast and bacteria were observed to grow together as a biofilm.<sup>[18]</sup> Notably, specific bacterial and fungal species showed significant associations, including a negative correlation between *Corynebacterium*

and *C. albicans* and *Candida parapsilosis*, indicating intricate interactions between fungi and bacteria.<sup>[18]</sup> For these reasons, the development of novel and efficient antifungal agents is required when designing a wound healing material.

AgNPs derived through green synthesis (G-AgNPs) have been shown to exhibit strong antibiofilm activity, and be effective against *E. coli*, *P. aeruginosa* and *S. aureus*, Gram negative bacteria<sup>[19]</sup> as well as pathogen fungal.<sup>[20]</sup> This contributes in the fight against growing epidemics of antibiotic and antifungal resistance whilst reducing post-surgical complications and prices for patients.<sup>[14]</sup>

In our recent study, we demonstrated the absence of in vitro cytotoxicity of G-AgNPs when incorporated within the eggshell membrane, showcasing their potential as a promising platform for wound healing applications, demonstrating a stronger microbial inhibitory effect when compared to commercial AgNPs products.<sup>[21]</sup>

Concerning that, this study describes a translational method for producing both collagen scaffolds and a frugal biomaterial – each fabricated with and without G-AgNPs. It explores the feasibility of creating potential wound healing materials through scalable, tunable and environmentally friendly procedures. Both materials are characterized as potential wound healing bionanocomposite materials with fungicidal activity. These materials offer a lower cost, mechanically strong, antimicrobial alternative compared to existing wound-dressing materials which can become a favorable place for microorganism colonization, resulting in increased microbial load and reduced rate of wound-healing.<sup>[22]</sup> Through this study, we aim to utilize green processes to manufacture collagen and agar/cellulose scaffolds incorporated with G-AgNPs and to investigate biocompatibility, mechanical, antimicrobial, and structural properties. The antifungal efficacy of both developed materials was assessed in vitro in accordance with ISO 16869:2008 standards, focusing on their effectiveness against *Cladosporium* spores. Although rare, *Cladosporium* is reported to cause severe skin diseases in humans.<sup>[16,23]</sup>

In addition to this, we also aim to understand the effects of G-AgNP incorporation into these biomaterials and correlate these to results obtained from biological and mechanical testing.

## 2 | MATERIALS AND METHODS

### 2.1 | Materials

Food grade agar, glycerol and Carboxymethylcellulose (CMC) were procured from Sigma–Aldrich, UK. Silver nanoparticles synthesized from natural ingredients were

acquired from Metalchemy Limited and produced using method outlined in patented process.<sup>[12]</sup> The pH of the provided solution is adjusted with 0.1 M HCL to a pH of 7.

### 2.2 | Preparation of films

#### 2.2.1 | Agar/G-AgNPs composite

For the preparation of agar/Ag composite films, 0.5–2 g of Agar powder (Sigma–Aldrich, UK) was dissolved in G-AgNPs solution (Metalchemy, UK) containing 0.5–1 g of glycerol (Sigma–Aldrich, UK) as a plasticizer and 0.4–1 g of CMC (Sigma–Aldrich, UK) while mixing vigorously for 30 minutes at 95°C and cast evenly onto a leveled metallic casting plate (20 × 30 cm), then dried for approximately 30 minutes at 70°C followed by 2 hours at 40°C in a convectional dehydrator. Once dried, the resultant film was peeled from the casting surface and stored at room temperature.

#### 2.2.2 | Collagen films and G-AgNP/collagen films

Acellular collagen gels were prepared in 24-well plates in accordance with an established protocol (10, 28). In brief, the following reagents were combined; 80% type I rat tail collagen (2 mg/mL<sup>-1</sup> protein in 0.6% acetic acid: First Link UK Ltd, UK), 10% of 10x concentration of Minimum Essential Medium (10X MEM; Gibco), 5.8% of neutralizing solution (HEPES Buffer with 1 M Sodium Hydroxide) and finally 4.2% cell culture media (Dulbecco's modified eagle's Medium with 10% Foetal bovine serum (FBS) and 1% Penicillin/streptomycin). The collagen mixture was produced on ice to prevent the collagen setting. Once formed, gels were incubated and allowed to set for 30 minutes at 37°C and 5% CO<sub>2</sub>. Following incubation, collagen hydrogels were dehydrated using layers of absorbent filter paper. A similar process is conducted for preparing AgNP collagen films. G-AgNPs were incorporated into the collagen mixture at the concentrations shown on Table 2. A schematic representation of the adopted procedure has been reported in Figure 1.

### 2.3 | Material characterization of samples

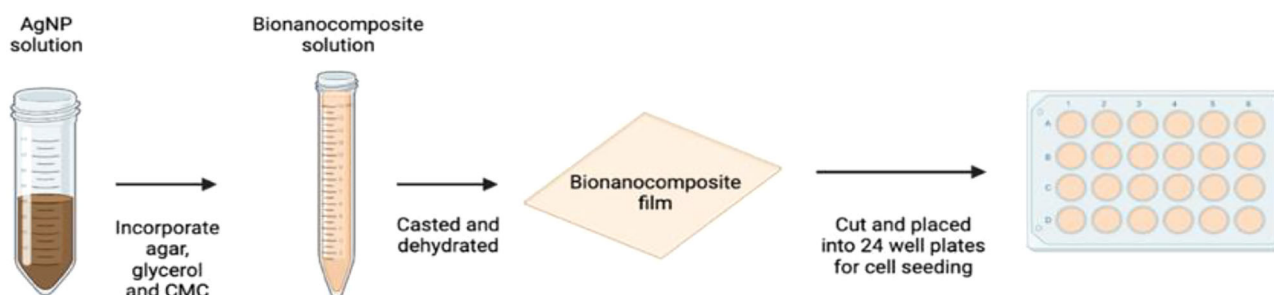
#### 2.3.1 | Nanoparticle characterization

In order to characterize the G-AgNP solution and quantify the concentration and distribution of nanoparticles,

TABLE 2 Name and composition of Collagen and Bioplastic samples (with and without G-AgNPs).

Sample	Name description	AgNPs composition (v/v%)
Col	Collagen film	0%
Col-4%AgNPs	Collagen film	4%
Bio	Bioplastic	0%
Bio-15%AgNPs	Ag Bionanocomposite	15%
Bio-30%AgNPs	Ag Bionanocomposite	30%

### Agar/AgNP Nanocomposite Film



### Collagen/AgNP Nanocomposite Film

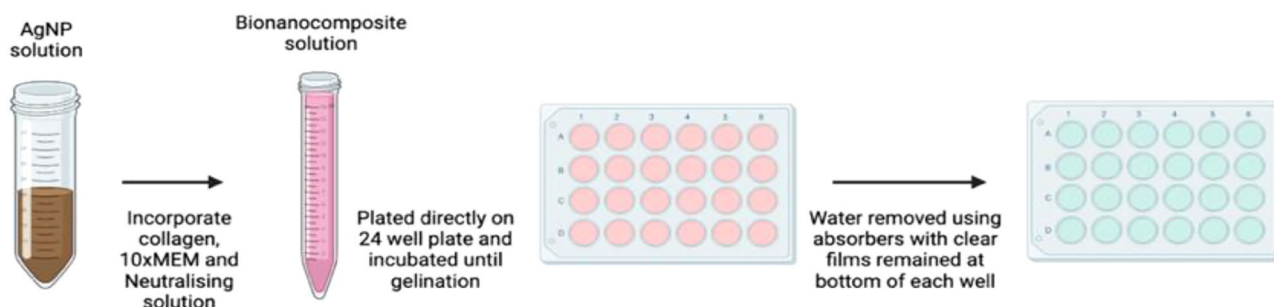


FIGURE 1 Visual diagram of methodology for preparing bionanocomposite and collagen films.

the UV-vis spectra were recorded on a Shimadzu UV-1900i spectrophotometer. 1 mL of G-AgNP solution was plated in 24 well plates and scanned in wavelength range 300–600 nm for the absorption spectra.

### 2.3.2 | Mechanical testing

Both ultimate tensile strength and elongation at break (%) were determined using the zwickiLine tensile tester from ZwickRoell (Ulm, Germany). The bioplastic control and bioplastic with G-AgNPs samples were cut into 5 mm wide dog-bone shapes of 38 mm length using a standardized punch. Each test sample was placed into the grips of testing apparatus set 12 mm apart and tested to failure at a speed of 10 mm/minute. Before testing,

the thickness of each sample was measured using digital vernier caliper. Data from the apparatus was interpreted by TestXpert II, Zwick Roell Group, Ulm, Germany which produced stress/strain curves for each material. Data from these curves was exported onto a Microsoft Excel spreadsheet where stress in MPa was calculated for each material.

The following formulas was used to calculate the ultimate tensile strength and elongation at break:

$$IfTS = Fmax/A0 \quad (1)$$

where,  $IfTS$  = tensile strength,  $Fmax$  = maximum force, and  $A0$  = initial surface area.

$$\text{Elongation} = \varepsilon = (\Delta/L) \times 100 \quad (2)$$

where,  $L$  = initial length,  $\Delta L$  = change in final length and initial length

### 2.3.3 | Antifungal activity

The antifungal activity of the bionanocomposites were assessed via the methodology presented in the International Standard ISO-16869:2008.<sup>[24]</sup> The antifungal activity of the bioplastic was analyzed against *Cladosporium* of domestic origin with initial concentration of  $\geq 5 \times 10^6$  spores/mL. Square film samples ( $10 \times 10$  mm) were placed in sterilized petri dishes in a nutrient-agar medium and incubated in Sciquip Incubator S-Series SQ-4615 at  $23 \pm 1^\circ\text{C}$  for 21 days. Bioplastic and Collagen samples without G-AgNPs were used as control with the same biological environment. Pictures of each petri dish were taken at regular intervals and inhibition zone was tracked using ImageJ software.

### 2.3.4 | Cell culture of human dermal fibroblast (HDF) cells

A human dermal fibroblast (HDF) cell line (Thermo Fisher Scientific – Waltham MA, USA) Catalogue number: C0135C) were used for this work. The cells were suspended in cell culture media (10% FBS, 1% penicillin/streptomycin) and incubated in T125 culture flasks at  $37^\circ\text{C}$  and 5%  $\text{CO}_2$ . The media was changed every 48 hours after initial culture until the HDF cells reached  $\sim 70\%$  confluence. Cells were dissociated from culture flasks using trypsin (0.5% with EDTA – Gibco), then re-suspended in culture media before centrifugation at 1500 rpm for 5 minutes. Post centrifugation, the cell pellet was resuspended in culture medium. Cell density was determined by trypan blue dye exclusion using a ThermoFisher Scientific Countess 3 FL Automated Cell Counter. HDF cells were seeded on the surface of samples at a density of 200,000 cells/mL. Seeded samples were then incubated at  $37^\circ\text{C}$  and 5%  $\text{CO}_2$  in base medium and investigated for adhesion and proliferation throughout 5 days of culture.

### 2.3.5 | In vitro metabolic activity assessment

To assess the metabolic activity of HDF cells seeded on both the bioplastic and collagen scaffolds, a 3-(4,5-dimethylthiazol-2-yl)-2,5-diphenyltetrazolium bromide tetrazolium (MTT) reduction assay was conducted. The MTT assay kit was obtained from Biotium and carried out as specified by the manufacturer. After cells were seeded onto bioplastic and collagen scaffold samples in respective 24-well plates, they were incubated at  $37^\circ\text{C}$ , 5%

$\text{CO}_2$  in base medium. The MTT assay was conducted at day 1, 2, 3 and 4. Each day, 50  $\mu\text{L}$  of MTT was added to each well containing 500  $\mu\text{L}$  of media. This was followed by incubation in the same conditions for 2 hours. Purple formazan crystals were dissolved using dimethyl sulfoxide (DMSO) and the absorbance was taken using an Infinite 200 Pro plate-reader device at 570 nm, and background at 630 nm. In addition to compare the absorbance of the bionanocomposite materials to a standard, the same number of cells seeded onto the scaffolds (200,000) were also seeded into a well containing media and incubated for the same amount of time. For each day the MTT assay was conducted on the biomaterials, it was also carried out on the respective cells in media that had been incubating for the same time. The equation below was used to obtain cellular metabolic activity/proliferation relative to cells in media, both seeded in a 24-well plate.

*% Net Change in Cellular Metabolic Activity/Proliferation*

$$= \frac{\text{Mean Abs}_{\text{Sample}}}{\text{Mean Abs}_{\text{Blank}}} - 1 \quad (3)$$

### 2.3.6 | Inverted phase contrast optical microscopy

An inverted phase microscope was used to visually examine morphology of HDF cells seeded upon the bionanocomposite materials. HDFs were cultured for a week to study the growth of cells on the materials.

### 2.3.7 | Scanning electron microscopy

Samples were fixed in 4% (PFA) (Fisher Scientific UK Ltd) for 20 minutes. The fixed samples were dehydrated using ascending concentrations of ethyl alcohol at 70%, 90%, and 100%. The samples were mounted on aluminum pin stubs and sputter coated with gold/palladium (Polaron E5000, Quorum Technology, UK) prior to being examined with the samples were analyzed using a Scanning Electron microscope (Zeiss Sigma 300VP).

The shape, size and distribution of the embedded G-AgNPs along with the porosity of the bionanocomposite samples and G-AgNPs integration were assessed using ImageJ software.

### 2.3.8 | Fluorescence microscopy

Fluorescence microscopy imaging was used to investigate cell adhesion and proliferation on collagen samples. After

1, 2 and 5 days of culture, collagen samples were all fixed with 4% PFA for 30 minutes then rinsed with PBS. Samples were immersed in 0.5% TritonX-100 for 30 minutes. After PBS rinsing, each sample was then stained with phalloidin (FITC- P5282.1MG: TRITC-P1951-1MG Sigma–Aldrich) 6-well) (1:1000) and kept in the dark for 45 minutes. Upon time, it was again rinsed with PBS before adding 1 drop of DAPI (VECTASHIELD with DAPI (H-1200 Vector Laboratories Inc) onto the sample and left for 15 minutes. They were then rinsed with PBS and imaged in the well plate by 20x using a Zeiss LSM 710 fluorescence microscope (Zeiss – Obercohen, Germany).

### 2.3.9 | Statistical analysis

All experimental measurements and analyses in this study were conducted using independently prepared samples to ensure the robustness and reliability of our findings.

The following equation was used to calculate the arithmetic mean:

$$\bar{x} = \frac{1}{n} \sum_{i=1}^n x_i \quad (4)$$

where,  $\bar{x}$ : arithmetic mean,  $n$ : number of values, and  $x_i$ : data set of values.

And the following equation was used to calculate the standard deviation:

$$\sigma = \sqrt{\frac{\sum (x_i - \bar{x})^2}{n}} \quad (5)$$

where,  $\sigma$ : standard deviation (SD),  $\bar{x}$ : arithmetic mean,  $n$ : number of values,  $x_i$ : data set of values.

Each experiment was performed in triplicate and the data were subsequently processed and analyzed using Microsoft Excel tools using Equations (4) and (5). Where appropriate, the results were provided with the mean ( $\bar{x}$ )  $\pm$  standard deviation (SD) values.

## 3 | RESULTS AND DISCUSSION

### 3.1 | Green silver nanoparticle characterization (G-AgNPs)

UV-vis spectrometry was first performed to characterize the G-AgNP solution. Silver nanoparticles are known to exhibit a distinctive surface plasmon resonance band in the range of 400–450 nm.<sup>[25]</sup> Figure 2 shows the characteristic peak maximum at around 400 nm which matches the silver nanoparticles SPR (Figure 2). A spherical geometry of

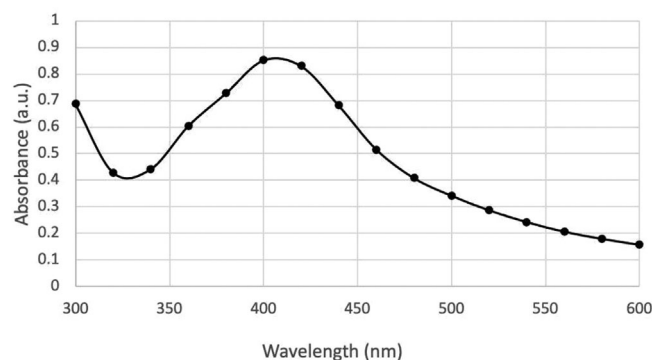


**FIGURE 2** UV-vis spectroscopy of G-AgNP solution suggesting spherical shape of nanoparticles exhibiting standard surface-plasmon resonance peak.

the particles as seen in literature is also indicated by the gaussian shape observed.<sup>[26]</sup>

The size and shape of the G-AgNPs were characterized by analyzing SEM images as seen in Figure 3A,B. Observed images showed spherical particles well dispersed and non-agglomerated under different magnifications at 20 and 80 k.

Size distribution analysis histogram shown in Figure 4 shows that the particle diameters are predominantly in between 20 and 25 nm with average diameter of 21.4 nm with a normal distribution. Spherical items are included for this analysis, and non-spherical items have been automatically excluded by adjusting the circularity coefficient ( $\Phi$ ) during image processing on ImageJ. This results in normal distribution of spherically shaped of G-AgNPs in the analysis.

### 3.2 | Bioplastic and collagen mechanical properties

Table 3 shows that the bioplastic scaffolds exhibit greater mean UTS, elongation at break and Young's Modulus measurements when compared to collagen. For example, the UTS for the bioplastic is >6 times greater than the standard value for collagen scaffolds, while still having similar average thickness. In addition to this, the extensibility of the bioplastic is a desirable characteristic of an optimal tissue scaffold, as it allows expansion, compression and contraction and healing of tissue – reducing the risk of constricting scar formation. Furthermore, the tunability through the use of G-AgNPs of bioplastic allows further manipulation of mechanical properties, depending on the use of the tissue scaffold – allowing the user to adapt the material and personalize its use. It has been shown that the addition of G-AgNPs increased the tensile strength by 15%, further highlighting the tunability of bioplastic materials – with

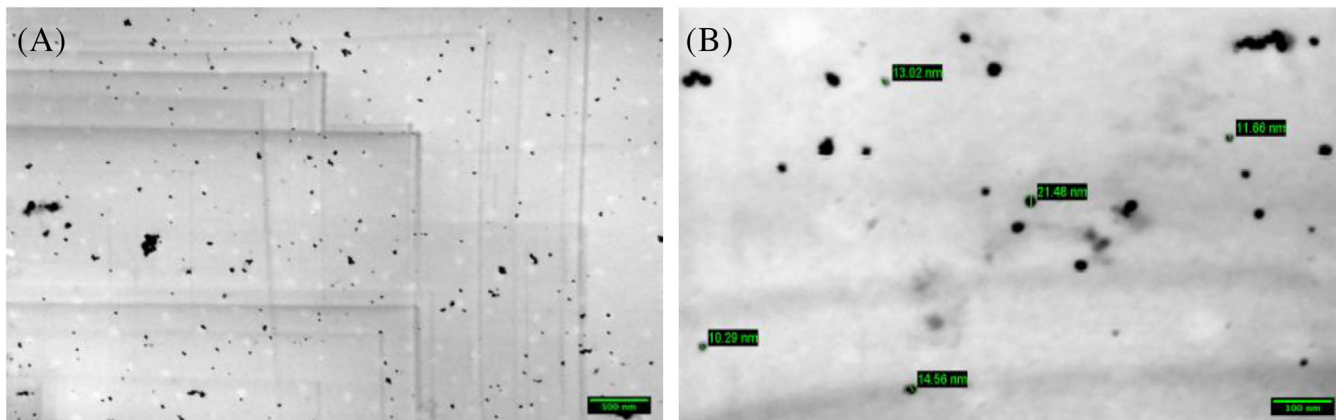


FIGURE 3 SEM image of G-AgNPs at (A) 20 KX and (B) 80 KX showing that nanoparticles are well distributed.

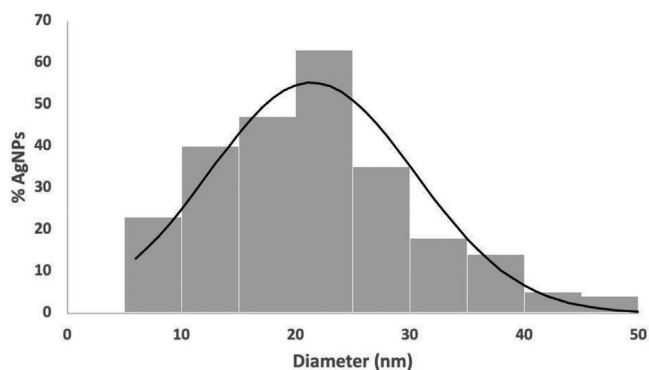


FIGURE 4 Histogram presenting size distribution of G-AgNPs as obtained through ImageJ analysis of SEM imaging. A bell-curve of best fit is drawn on the histogram to indicate normal distribution with average nanoparticle diameter of  $\bar{x} = 21.4$  nm.

TABLE 3 Summary of mechanical measurements and testing of bioplastic (thickness, ultimate tensile strength, % elongation at break and Young's modulus). The collagen scaffold average thickness and respective mechanical properties were obtained from literature using the same material produced through the standard RAFT process.<sup>[28]</sup>

	Bio +/- S.D	Col +/- S.D
Average thickness (mm)	0.168 +/- 0.122	0.094 +/- 13
UTS (MPa)	3.860 +/- 1.891	0.60 +/- 0.1
% Elongation at break	14.935 +/- 0.594	55.0 +/- 13.8
Young's modulus (MPa)	0.422 +/- 0.237	1.3 +/- 0.3

material strength increasing with the concentration of G-AgNPs.<sup>[27]</sup> Despite an increase in toughness, a reduction in % elongation when increasing quantities of G-AgNPs were added.<sup>[27]</sup>

Bioplastic and collagen mechanical properties can therefore be tuned by the addition of G-AgNPs to fit the

required application for the patient delivering for a more personalized treatment adapting to patient needs.

### 3.3 | Biomaterial structural analysis

It is shown in Figure 5A,B the control bioplastic revealed a smooth surface without visible pores and any surface defects at a magnification of 5 k. The absence of pores even at 20 k magnification suggests a smooth and uniform surface structure. Figure 5B,C shows the surface of Bio-30%AgNPs for which a higher surface roughness is observed. At magnification of 5 and 10 k, G-AgNPs are observed on the surface being homogeneously anchored on the matrix. This further confirms the successful embedding of G-AgNPs on the biopolymer matrix. The incorporation of silver nanoparticles induced formation of pores in bioplastic as shown at 5 k magnification. A porous microstructure could lead to better support of cell growth by allowing adequate diffusion of nutrients and inter-matrix cellular penetration.<sup>[29]</sup>

An average pore size of 19.340 nm was calculated through image analysis on Image J software which is similar to the average size of the G-AgNPs, indicating the contributive role of nanoparticle content in the porosity of the substrate matrix (Figure 6).

A porous structure can also be beneficial in different applications such as bone tissue scaffolds to encourage angiogenesis.<sup>[30]</sup> The tunability of the bioplastic allows it to be easily customized for different application or patient needs, offering a competitive edge over current use of synthetic meshes and collagen hydrogels which have limited adaptability.<sup>[14]</sup>

SEM images were taken to analyse the morphology of the collagen scaffolds – both Col and Col-4%AgNPs. As shown by Figures 7 and 8, both samples presented with a highly porous surface structure at magnifications of 5, 10,

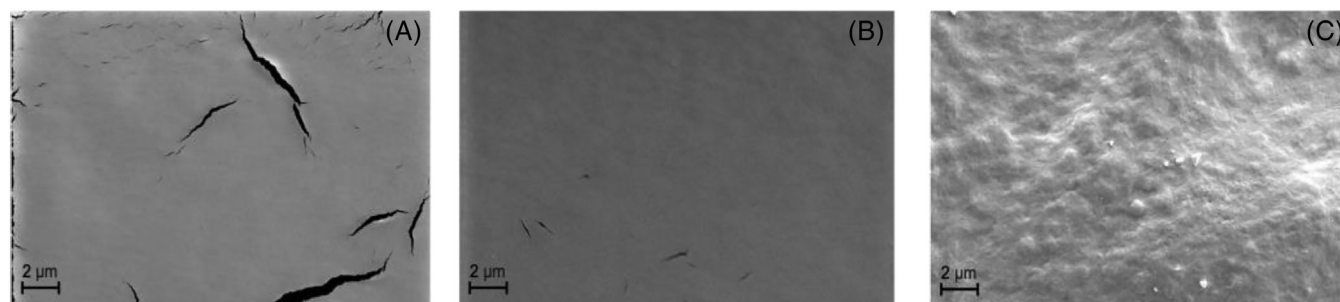


**FIGURE 5** A, SEM image of Bio at 5 k. B, SEM image of Bio-15%AgNPs at 5 k. C, SEM image of Bio-30%AgNPs at 5 k. G-AgNPs are well integrated in sample B with no major agglomeration visible. Less surface cracking is observed between Bio-15%AgNPs and Bio-30%AgNPs versus control bioplastic suggesting a better structural integrity conferred by G-AgNPs. At higher concentrations of G-AgNPs exhibits a rougher surface which could benefit cell adhesion and proliferation.

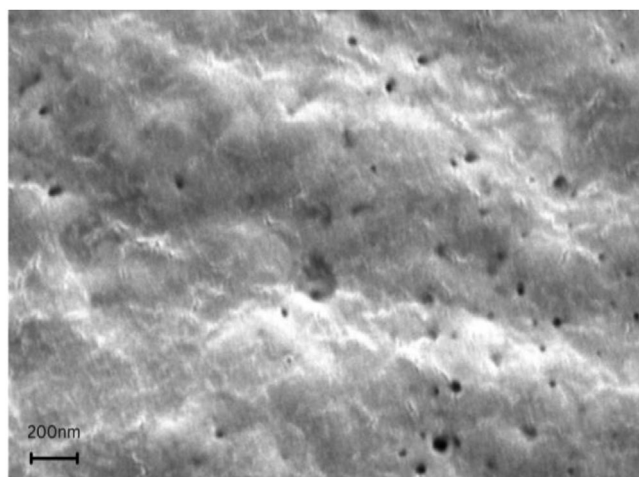


**FIGURE 6** SEM image of Bio-30%AgNPs at 40 k showing nanoporous structures on the surface of similar diameter of G-AgNPs suggesting a potential porophore function in biomaterial formation.

and 20 k. However, it could be observed that the addition of G-AgNPs with Col-4%AgNPs resulted in similar porosity as shown at 10 k magnification when compared to the same magnification for Col – with larger and denser pores being found. On Figure 8, Col-4%AgNPs presents the anchorage of G-AgNPs which can be observed on the surface and bulk of the collagen scaffold, as highlighted in red. This confirms the presence of G-AgNPs, and suggests that the G-AgNPs are well-embedded within the matrix and are acting to enhance the material. These results are in line with current literature adding G-AgNPs to collagen hydrogels – for example, a recent study found that their SEM images showed that addition of G-AgNPs did not change the fibrillar structure of their collagen hydrogels, and instead remained attached to the fibrils without increasing surface porosity at 200 nm scale.<sup>[7]</sup> SEM imaging has demonstrated that our G-AgNPs are able to anchor effectively

within the matrix of bioplastic and collagen scaffolds as well as homogeneously distributing on the materials.

### 3.4 | Antimicrobial activity of collagen and bioplastic G-AgNPs scaffolds

In order to investigate the antifungal properties of developed systems, Col-4%AgNPs and Bio-30%AGNPs (containing 30% AgNPs), were tested against *Cladosporium* spores according to ISO-16869:2008 (11) procedure for evaluating the effectiveness of fungistatic compounds in plastics formulations. While rare, *Cladosporium* is known to cause severe skin diseases in humans and it represents an optimal model fungal for our study. Figure 9 shows antifungal activity of developed materials against *Cladosporium* spores over 21-day period.

Both graphs undergo exponential reduction followed by linear reduction in inhibition zone over the first 4 days, and then begin to stabilize when the diameter of the inhibition zone is similar to the diameter of the material containing G-AgNPs. Despite Col-4%AgNPs containing 7.5 times lower concentration of G-AgNPs, it demonstrates similar performance in inhibiting the growth of *Cladosporium* compared to Bio-30%AgNPs. Also, this means that the minimum inhibitory concentration of G-AgNPs is not reached even at 4% G-AgNPs against *Cladosporium*. While Bio-30%AgNPs stabilizes at an inhibition zone of around 13.3 mm at the end of the test, Col-4%AgNPs displays an inhibition zone of 11.2 mm at the same time – proving the similarity in antimicrobial efficacy of both materials.

The first observation of fungi in the control bioplastic samples was on day 3. However, all three samples had clear fungal growth on day 4. In comparison, the G-AgNPs embedded bioplastic only showed penetration signs of fungi activity on average after 10 days, an improvement of 233%. Therefore, the G-AgNPs embedded in the

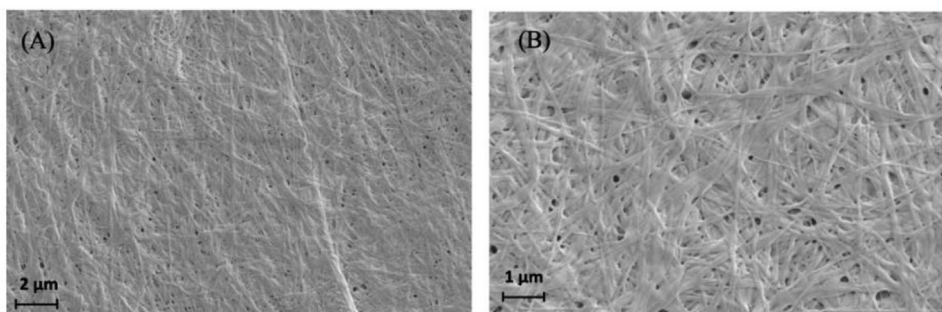


**FIGURE 7** Collagen control SEM image at 5 k magnification (A) and 10 k magnification (B) exhibiting fibrillar and porous structure produced through RAFT method.

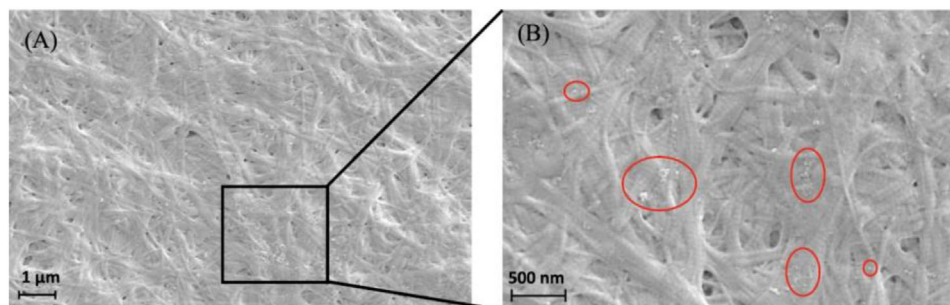


**FIGURE 8** Col-4%AgNPs SEM image at 10 k magnification (Right) and 20 k magnification (Left). G-AgNPs highlighted in red were identified on the sample with good surface anchorage without impacting the collagen fibrillar structure.

biomaterials improve its resistance to the growth of *Cladosporium*, providing the nano-enhanced bioplastic anti-fungal properties. With regards to the control collagen (Col), all samples were fully covered by the *Cladosporium*. Over the course of the 21 days of testing, Col-4%AgNPs did not become fully penetrated by *Cladosporium*, however showed first signs of penetration on day 7 – giving an improvement of 75%. The signs of microbial penetration observed on the Col-4%AgNPs films remained the same size from day 7 to day 21 of testing, suggesting that the G-AgNPs inhibit growth of *Cladosporium* even at 4% G-AgNPs concentration – as presented on in the Supplementary information (Figure SI-2). The same pattern was observed for the Bio-30%AgNPs (Figure SI-1) films, with mould growth on the film remaining at the same size over the course of testing as shown in the [Supplementary information](#).

### 3.5 | Cellular growth and metabolic activity in G-AgNPs scaffolds

As shown on Figure 10A, at Day 4, Bio-30%AgNPs indicated the greatest net change in cellular metabolic activity of all samples at over 50%. All samples containing G-

AgNPs exhibited a general trend of increase in net cellular metabolic activity over 4 days of incubation. This suggests that HDF cells require a period of acclimatization and stabilization to the G-AgNPs before they act to improve cell proliferation and metabolic activity.

Figure 10B shows a measured difference between Col and Col-4%AgNPs in metabolic cell activity, with Col-4%AgNPs having over 1.3x net change in cellular metabolic activity on day 4 when compared to Col. In addition to this, Col-4%AgNPs shows a steady increase in cellular metabolic activity over the course of incubation, while Col shows more of a cyclical pattern, decreasing and increasing on alternate days.

This suggests that the incorporation of G-AgNPs into collagen, even at a low concentration of 4%, interacts within the collagen scaffold matrix and HDF cells as demonstrated by the improved cellular metabolic activity measurements observed over the 4 days of testing. However, Col-4%AgNPs showed net cellular metabolic activity of  $-10.8\%$  on Day 1, while no change in cellular metabolic activity was observed for the control collagen. This initial reduction in cellular metabolic activity could be due to the same reason as the bioplastics shown in Figure 10A, with the HDF cells requiring a period of acclimatization to the G-AgNPs.<sup>[31]</sup>

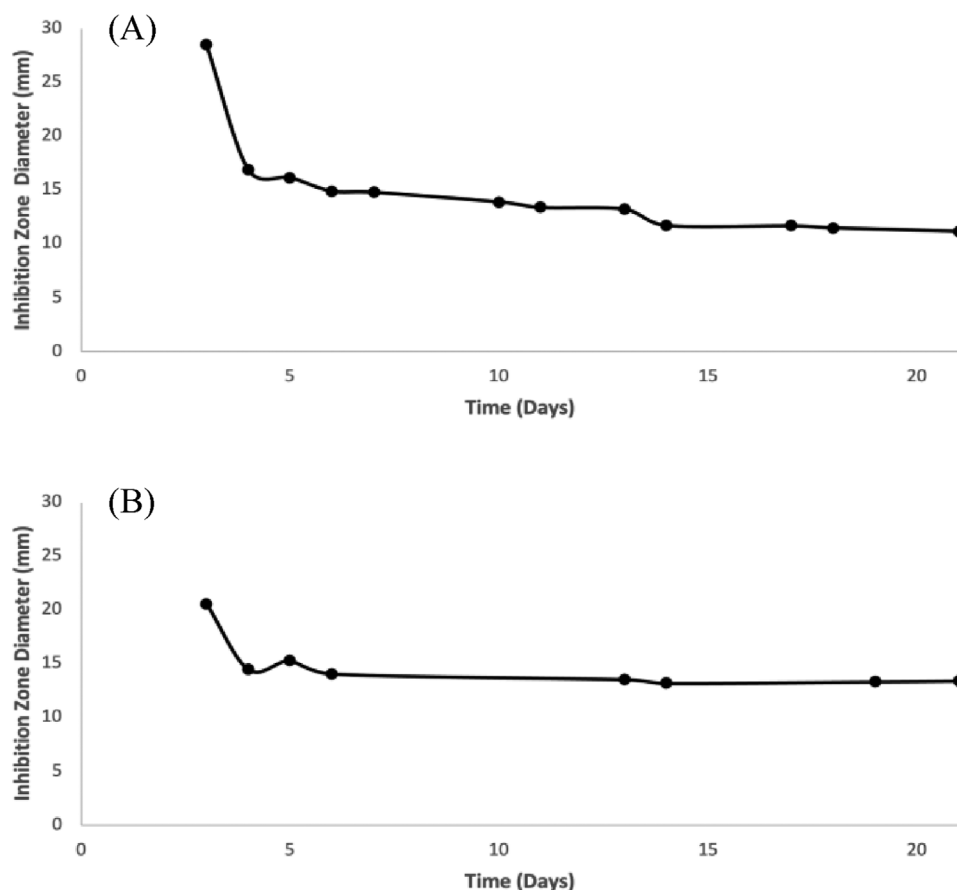


**FIGURE 9** A, Col-4%AgNPs antimicrobial testing. B, Bio-30%AgNPs antimicrobial testing over 21 days against *Cladosporium* spores following ISO-16869:2008. Similar trends are observed for both bionanocomposites despite major difference in G-AgNPs concentration.

These positive results from the MTT assay suggest that HDF cells respond well to G-AgNPs, incorporated within various materials – resulting in increased metabolic activity of viable cells. As there is an increase observed for metabolic activity over the 4 days of testing, it can be said that the addition of the silver nanoparticles does not result in great cytotoxicity, as the MTT assay is a marker for metabolic activity of viable cells.<sup>[21]</sup> This behavior can translate to the implementation of effective tissue scaffolds which result in an increased rate of healing, as cells have been shown to adapt metabolism and upregulate certain signaling pathways as they proliferate, and hence induce pro-fibrotic changes within tissues and cause remodeling.<sup>[32]</sup>

Light microscopy revealed that HDF cells attached and proliferated during culture on both bioplastics and collagen bionanocomposites. As shown on Figure 11, cells growing on agar/cellulose films demonstrated a more branched morphology which could be due to the complex polysaccharide structure allowing for strong embedment. High cell coverage over films was observed on all samples with high level of confluence especially for Bio-30%AgNPs and Col-4%AgNPs which indicates good biocompatibility of

the films. Fixed bioplastic samples Bio, Bio-15%AgNPs and Bio-30%AgNPs presented well adhered elongated HDF cells attached to the material.

Similarly, within the collagen matrix, we observed proliferative cell growth over the experimental period using fluorescence microscopy. Both the fixed control and nanoparticle-incorporated samples on day 5 demonstrated cell adhesion. Immunofluorescence staining for actin (in red) and nucleus (in blue) was employed to further monitor cell attachment and spreading on the film surface. As illustrated in Figure 12, the seeded cells exhibited extensive cytoskeletal structures, even in the presence of silver nanoparticles. These findings are consistent with our previous work where we demonstrated the presence of G-AgNPs further promoting cell growth.<sup>[21]</sup> MTT analysis, revealing a more pronounced cytoskeletal structure with increased fluorescence in the imaging of Col-4%AgNPs compared to the collagen control. This result has been attributed to the presence of G-AgNPs within the biocomposite, as previously demonstrated in our work where a strong pro-angiogenic activity has been observed when combining the NPs within eggshell membrane.<sup>[21]</sup> Indeed, enhanced cell adhesion to the substrate contributes to

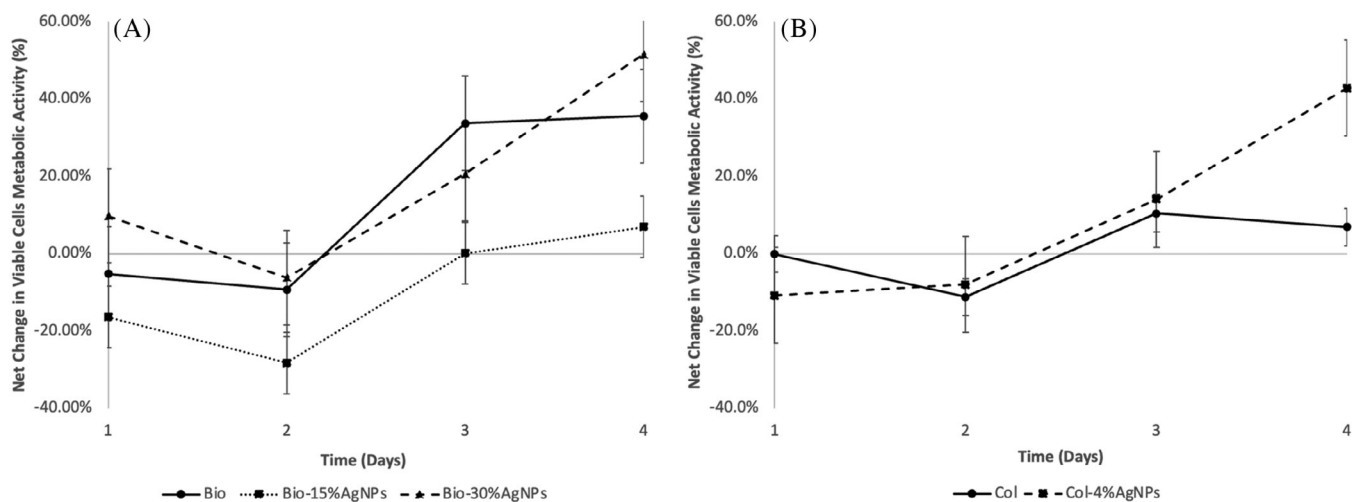


**FIGURE 10** Net change in viable cellular metabolic activity derived from MTT assay in %. A, Bioplastic scaffolds. B, Collagen Scaffolds when compared to cellular metabolic activity of cells cultured on well plate.

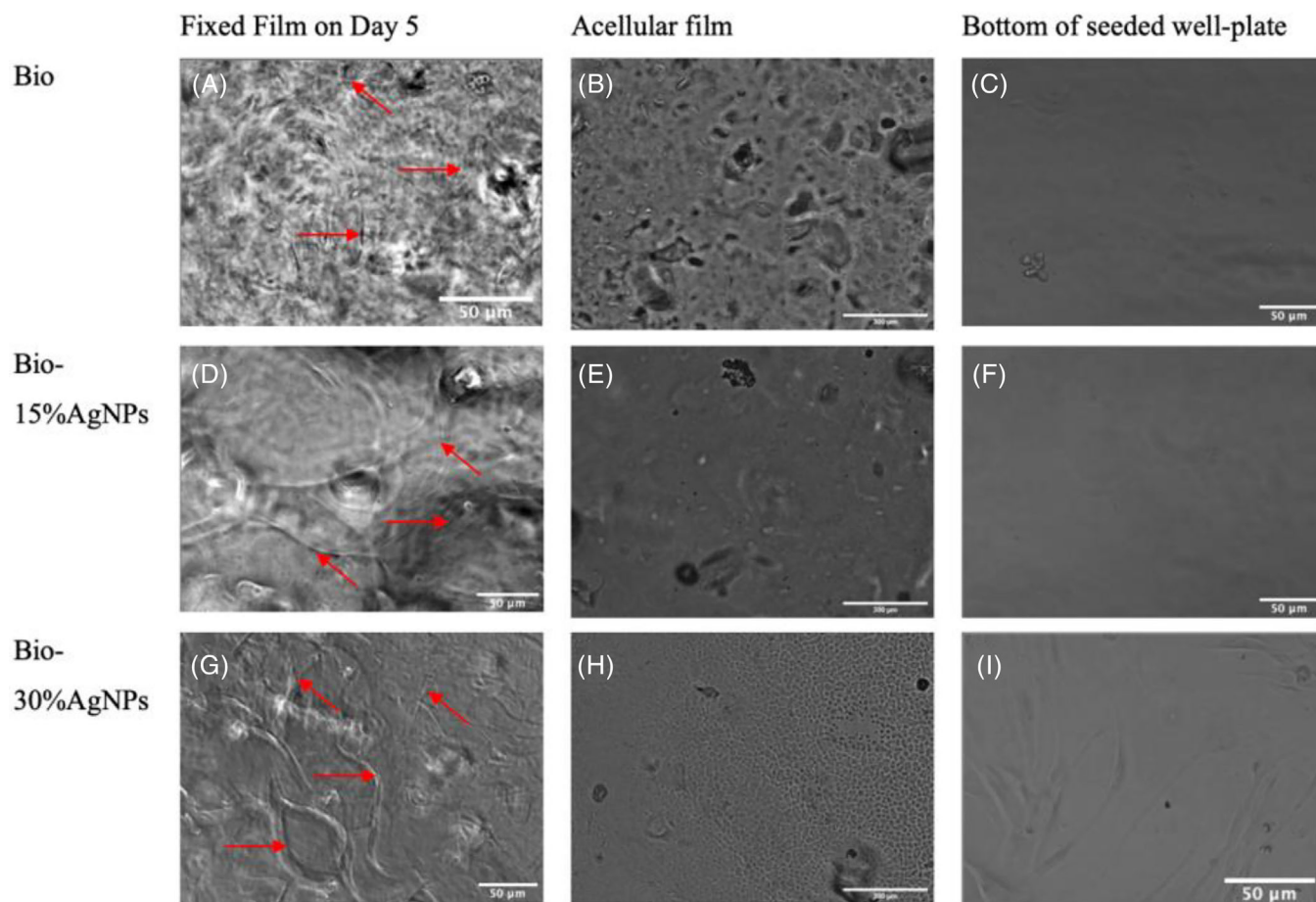


**FIGURE 11** Light Microscopy imaging of bioplastics on fixed day 5 samples at 5 k magnification (Bio = a, Bio-15%AgNPs = d, Bio-30%AgNPs = g), acellular samples (Bio = B, Bio-15%AgNPs = E, Bio-30%AgNPs = H) and well plate after removal of fixed sample (Bio = C, Bio-15%AgNPs = F, Bio-30%AgNPs = I). Cells can be observed on fixed bioplastic films (A, D, G) with no cells visible on acellular films when compared (B, E, H). The bottom of seeded well-plates exhibited no visible HDF cell presence (C, F) aside for test sample (I). Proliferation of HDF cells.

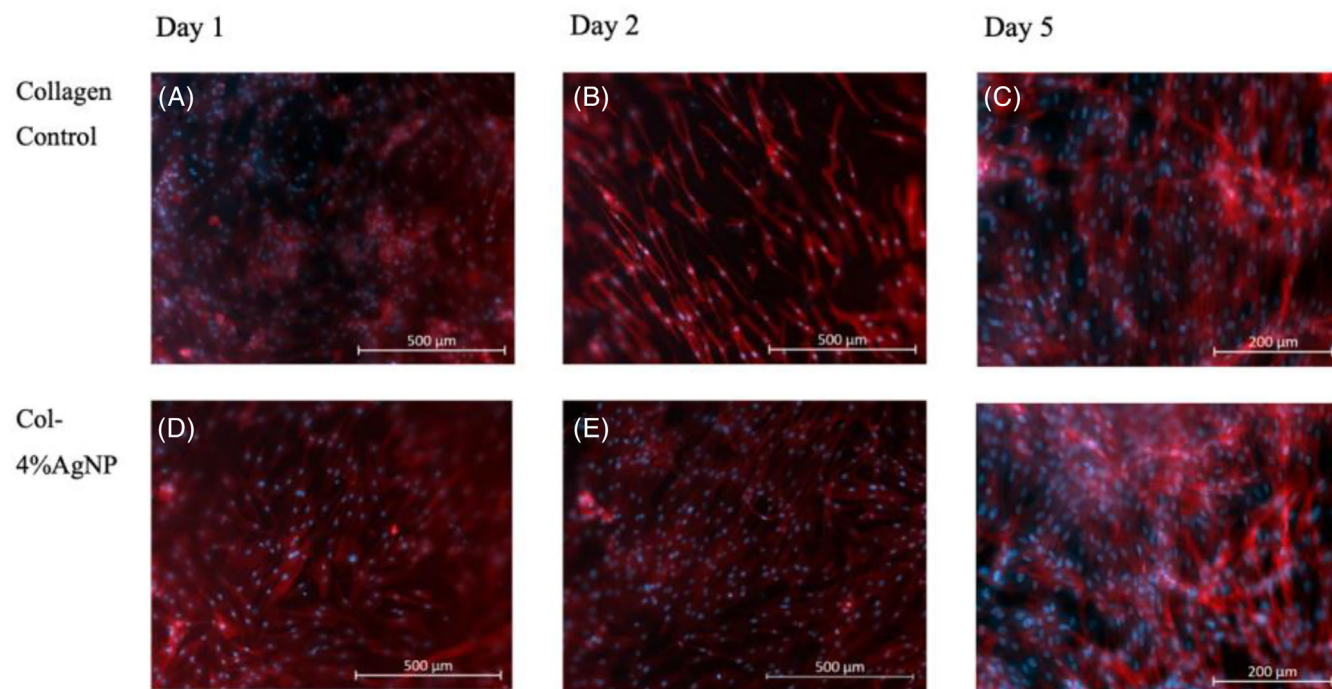


**FIGURE 12** Fluorescence imaging (Phalloidin shown by red staining with DAPI shown by blue staining) of Col-C and Col-AgNP on fixed samples on day 1 (Col = A, Col-4%AgNPs = D), 2 (Col = B, Col-4%AgNPs = E), and 5 (Col = c, Col-4%AgNPs = F).

improved proliferation. Similar mechanisms have been described in oral mucosa cells exposed to silica, titanium, and hydroxyapatite nanoparticles.<sup>[32]</sup> Moreover, MTT assay and microscopy results indicate that both agar bioplastic and collagen groups did not negatively impact cell growth in the presence of G-AgNPs, confirming their biocompatibility. Bio-30%AgNPs and Col-4%AgNPs exhibited the most significant promotion of cell growth. This could be attributed again to G-AgNPs' ability to activate eNOS and induce NO-dependent cell proliferation.<sup>[33]</sup> Additionally, previous studies have shown that AgNPs can modulate collagen alignment, aiding cell proliferation for wound healing.<sup>[34]</sup> Similarly, in this case, cells on films incorporated with G-AgNPs appeared more confluent than their respective control counterparts, suggesting that both agar and collagen films are biocompatible and could facilitate wound healing processes.

#### 4 | CONCLUSIONS

The green synthesis route used in this study allows for the production of non-toxic silver nanoparticles suitable for human contact applications at a fraction of market price, approximately x5–10 lower than equivalent AgNPs.<sup>[12]</sup> Thus, the incorporation of green silver nanoparticles into polymers is an effective method to enhance antifungal properties of tissue scaffolds. The G-AgNPs used in our

study were shown through UV spectroscopy to have particle diameters between 20 and 25 nm with an average diameter of 21.401 nm. Small AgNPs (<10 nm) have been shown to exhibit cytotoxicity when exposed to human lung cells, suggesting that G-AgNPs in this study are optimal in size in order to maximize antimicrobial activity, while posing low risk for toxicity.<sup>[35]</sup>

Comparing agar and collagen-based G-AgNP film, both bionanocomposites demonstrated increased cell metabolic activity confirming G-AgNP's ability to promote cell growth. Viable cell metabolic activity derived from in vitro MTT assay absorbance values showed that Col-4%AgNPs and Bio-30%AgNPs had a 42.9% and 51.6% increase in metabolic activity respectively compared to control on day 4. Preliminary in vitro antifungal investigation against model fungal spores, expand the potential applications of the developed systems and in particular of G-AgNPs, which have so far been primarily used in antibacterial devices.

Concerning their mechanical properties, while collagen scaffolds offer greater water stability, the agar/collagen scaffolds offer significantly improved mechanical properties, making it ideal for wound-dressings that cover large areas due to the increased extensibility and tensile strength.

Future studies will be devoted to exploring and characterizing the properties of G-AgNPs bionanocomposite materials in different environments, with the aim of being

commercialized for use in wound-healing applications confirming their biodegradability and their ability to promote wound enclosure through wound healing scratch assays.

While our study focused on HDF cells, further investigations will encompass other cell types to validate biocompatibility, support prospective of more complex in-vivo studies, and assess efficacy against model pathogenic bacteria for its feasibility for clinical applications.

## NOMENCLATURE

AgNPs	silver nanoparticles
Bio	bioplastic scaffold (Agar-Cellulose)
Bio-15%AgNPs	bioplastic scaffold (Agar-Cellulose) with 15% 10 mg mL <sup>-1</sup> AgNP Solution Adjusted at pH 7
Bio-30%AgNPs	bioplastic scaffold (Agar-Cellulose) with 30% 10 mg mL <sup>-1</sup> AgNP Solution Adjusted at pH 7
Col	collagen scaffold
Col-4%AgNPs	collagen scaffold with 4% 10 mg mL <sup>-1</sup> AgNP Solution Adjusted at pH 7
G-AgNPs	green silver nanoparticles obtained through green synthesis (environmentally-friendly and non-toxic manufacturing method)
SI	Supplementary information

## ACKNOWLEDGMENTS

We acknowledge that this project was funded through the Materials and Manufacturing in Healthcare Innovation Network (MMHIN) award from University College London.

## CONFLICT OF INTEREST STATEMENT

Federico Trotta is an employee of Metalchemy Limited. Alna Dony and Monica Mok were employees of Metalchemy Limited. However, all funding for this project was awarded from MMHIN competition and financed independently from Metalchemy Limited. Metalchemy limited supplied green silver nanoparticles for the project. All experimental work was carried out in UCL laboratories and results reviewed independently from UCL researchers from Dr. Kureshi's group. Prof. Shervanthi Homer-Vanniasinkam is a scientific advisor of Metalchemy Limited.

## DATA AVAILABILITY STATEMENT

The raw/processed data required to reproduce these findings cannot be shared at this time as the data also forms part of an ongoing study.

## ORCID

Federico Trotta  <https://orcid.org/0000-0002-9170-2029>  
 Alvena Kureshi  <https://orcid.org/0000-0002-9738-8659>

## REFERENCES

1. C. K. Sen, *Adv. Wound Care* **2021**, *10*, 281.
2. J. F. Guest, N. Ayoub, T. McIlwraith, I. Uchegbu, A. Gerrish, D. Weidlich, K. Vowden, P. Vowden, *Int. Wound J.* **2017**, *14*, 322.
3. X. Zhu, M. M. Olsson, R. Bajpai, K. Järbrink, W. E. Tang, J. Car, *Int. Wound J.* **2022**, *19*, 1121.
4. U. Nation. THE 17 GOALS—Sustainable Development. Available online: <https://sdgs.un.org/goals>
5. R. Rendón-Villalobos, M. A. Lorenzo-Santiago, R. Olvera-Guerra, C. A. Trujillo-Hernández, *Polimeros* **2022**, *32*, 3.
6. C. Helary, M. Zarka, M. M. Giraud-Guille, *J. Tissue Eng. Regen. Med.* **2012**, *6*, 225.
7. P. E. Antezana, S. Municoy, C. J. Pérez, M. F. Desimone, *Antibiotics* **2021**, *10*, 3.
8. J. Su, J. Li, J. Liang, K. Zhang, J. Li, *Life* **2021**, *11*, 1.
9. B. Bhattacharai, Y. Zaker, T. P. Bigioni, *Curr. Opin. Green Sustain. Chem.* **2018**, *12*, 91.
10. D. Fuad, R. Fitrianiingsih, N. Mufti, A. Fuad, *AIP Conf. Proc.* **2014**, *1589*.
11. S. Gurunathan, K. Kalishwaralal, R. Vaidyanathan, D. Venkataraman, S. R. K. Pandian, J. Muniyandi, N. Hariharan, S. H. B. Eom, *Colloids Surfaces B Biointerfaces* **2009**, *74*, 328.
12. F. Trotta, *Composit. Methods* **2022**, GB2598715A.
13. A. Masri, A. Anwar, D. Ahmed, R. B. Siddiqui, M. R. Shah, N. A. Khan, *Antibiotics* **2018**, *7*, 1.
14. D. Kim, S. J. Kwon, X. Wu, J. Sauve, I. Lee, J. Nam, J. Kim, J. S. Dordick, *ACS Appl. Mater. Interfaces* **2018**, *10*, 13317.
15. L. J. Mendez-Tovar, *Clin. Dermatol.* **2010**, *28*, 185.
16. Y. B. Zhou, P. Chen, T. T. Sun, X. J. Wang, D. M. Li, *Mycopathologia* **2016**, *181*, 567.
17. A. R. Magray, S. Hafeez, B. A. Ganai, S. A. Lone, G. J. Dar, F. Ahmad, P. Siriyappagoudar, *Microb. Pathog.* **2021**, *151*, 104715.
18. Z. Xu, H. C. Hsia, *Ann. Plast. Surg.* **2018**, *81*, 113.
19. P. Singh, S. Pandit, C. Jers, A. S. Joshi, J. Garnæs, I. Mijakovic, *Sci. Rep.* **2021**, *11*, 12619.
20. A. H. Hashem, E. Saied, B. H. Amin, F. O. Alotibi, A. A. Al-Askar, A. A. Arishi, F. M. Elkady, M. A. Elbahnasawy, *J. Funct. Biomater.* **2022**, *13*, 5.
21. R. A. Mensah, F. Trotta, E. Briggs, N. S. Sharifulden, L. V. B. Silva, Z. Keskin-erdogan, S. Diop, A. K. Kureshi, D. Y. S. Chau, *J. Funct. Biomater.* **2023**, *14*, 450.
22. X. Ding, Q. Tang, Z. Xu, Y. Xu, H. Zhang, D. Zheng, S. Wang, Q. Tan, J. Maitz, P. K. Maitz, S. Yin, Y. Wang, J. Chen, *Burn. Trauma.* **2022**, *10*, 5.
23. A. M. Elgorban, A. E. R. M. El-Samawaty, O. H. Abd-Elkader, M. A. Yassin, S. R. M. Sayed, M. Khan, S. Farooq Adil, *Saudi J. Biol. Sci.* **2017**, *24*, 1522.
24. Plastics – Assessment of the Effectiveness of Fungistatic Compounds in Plastics Formulations (ISO 16869:2008). Available online: <https://www.iso.org/standard/45066.html>
25. A. Y. Vasil'kov, R. I. Dovnar, S. M. Smotryn, N. N. Iaskevich, A. V. Naumkin, *Antibiotics* **2018**, *7*, 14.

26. A. Almatroudi., *Open Life Sci.* **2020**, *15*, 819.
27. Z. Yu, W. Wang, R. Dhital, F. Kong, M. Lin, A. Mustapha, *Colloids Surfaces B Biointerfaces* **2019**, *180*, 212.
28. A. K. Kureshi, A. Afoke, S. Wohlert, S. Barker, R. A. Brown, *Biomech. Model. Mechanobiol.* **2015**, *14*, 1255.
29. A. Samourides, L. Browning, V. Hearnden, B. Chen, *Mater. Sci. Eng. C.* **2020**, *108*, 110384.
30. E. Petrovova, M. Giretova, A. Kvasilova, O. Benada, J. Danko, L. Medvecký, D. Sedmera, *ALTEX* **2019**, *36*, 121.
31. J. Zhu, C. B. Thompson, *Physiol. Behav.* **2019**, *176*, 139.
32. J. Franková, V. Pivodová, H. Vágnerová, J. Juráňová, J. Ulrichová, *J. Appl. Biomater. Funct. Mater.* **2016**, *14*, e137.
33. B. M. Carlson, *Eur. J. Transl. Myol.* **2014**, *24*, 5.
34. K. H. L. Kwan, X. Liu, M. K. T. To, K. W. K. Yeung, C. M. Ho, K. K. Y. Wong, *Nanomed. Nanotechnol. Biol. Med.* **2011**, *7*, 497.
35. A. R. Gliga, S. Skoglund, I. Odnevall Wallinder, B. Fadeel, H. L. Karlsson, *Part. Fibre Toxicol.* **2014**, *11*, 11.

## SUPPORTING INFORMATION

Additional supporting information can be found online in the Supporting Information section at the end of this article.

**How to cite this article:** F. Trotta, A. Dony, M. Mok, A. Grillo, T. Whitehead-Clarke, S. Homer-Vanniasinkam, A. Kureshi, *Nano Select* **2023**, *1*. <https://doi.org/10.1002/nano.202300087>